ELSEVIER

Journal of Hazardous Materials B136 (2006) 747–756

Journal of Hazardous Materials

www.elsevier.com/locate/jhazmat

Development of a double-layered ceramic filter for aerosol filtration at high-temperatures: The filter collection efficiency

Normanda L. de Freitas [a], José A.S. Gonçalves [a], Murilo D.M. Innocentini [b], José R. Coury [a,*]

[a] *Chemical Engineering Department, Federal University of São Carlos, Via Washington Luiz, km 235, 13565-905 São Carlos, SP, Brazil*
[b] *Chemical Engineering Department, University of Ribeirão Preto, Av. Costábile Romano, 2201 Ribeirânia, 14565-380 Ribeirão Preto, SP, Brazil*

Received 7 October 2005; received in revised form 22 December 2005; accepted 11 January 2006
Available online 8 February 2006

Abstract

The performance of double-layered ceramic filters for aerosol filtration at high temperatures was evaluated in this work. The filtering structure was composed of two layers: a thin granular membrane deposited on a reticulate ceramic support of high porosity. The goal was to minimize the high pressure drop inherent of granular structures, without decreasing their high collection efficiency for small particles. The reticulate support was developed using the technique of ceramic replication of polyurethane foam substrates of 45 and 75 pores per inch (ppi). The filtering membrane was prepared by depositing a thin layer of granular alumina–clay paste on one face of the support. Filters had their permeability and fractional collection efficiency analyzed for filtration of an airborne suspension of phosphatic rock in temperatures ranging from ambient to 700 °C. Results revealed that collection efficiency decreased with gas temperature and was enhanced with filtration time. Also, the support layer influenced the collection efficiency: the 75 ppi support was more effective than the 45 ppi. Particle collection efficiency dropped considerably for particles below 2 μm in diameter. The maximum collection occurred for particle diameters of approximately 3 μm, and decreased again for diameters between 4 and 8 μm. Such trend was successfully represented by the proposed correlation, which is based on the classical mechanisms acting on particle collection. Inertial impaction seems to be the predominant collection mechanism, with particle bouncing/re-entrainment acting as detachment mechanisms.

Keywords: Gas cleaning; High temperature filtration; Collection efficiency; Ceramic filters

1. Introduction

Hot gas filtration has become increasingly important in cogeneration plants employed to provide heat, electricity or power. In such technologies based on gasification, biomass combustion and waste incineration processes, the flue gases must be previously cleaned to avoid damage to downstream equipments or components and also to meet environmental regulations [1–3].

There are several technologies for conventional gas cleaning, and the correct choice depends on the features of the process and the nature of the pollutant. In hot-gas based plants, however, the hostile atmosphere that contains small particles and frequently toxicant gaseous components, restrains the available options. Fabric filters and wet scrubbers demand the cooling of the gaseous stream, making unfeasible the recovery of energy, in this case the major product of the process. Cyclones can withstand high temperatures and are relatively cheap and easy to operate, but their particle collection efficiency is low for particles smaller than 10 μm, hardly meeting the rigorous emission regulations [4]. Electrostatic precipitators, on the other hand, are very efficient for small particles and can operate at high temperatures, but they are expensive and therefore unfeasible for small-scale plants [2].

The ability to withstand temperatures above 500 °C with high efficiency has made ceramic filters one of the most successful technologies for hot gas cleaning in the past 20 years. It has been shown to be an interesting alternative for a number of applications. For example, in diesel particulate control, ceramic filters coupled with carbon combustion catalysts have been successfully used [5–8]. Ceramic filters have also been used for hot gas cleaning in pressurized fluidized bed combustors [9–11] and in methanol and hydrogen production from biomass [12].

Ceramic filters for hot gas cleaning can be roughly divided in two main categories according to the structure of their

* Corresponding author. Tel.: +55 16 3351 8440; fax: +55 16 3351 8266.
E-mail address: jcoury@power.ufscar.br (J.R. Coury).

0304-3894/$ – see front matter © 2006 Elsevier B.V. All rights reserved.
doi:10.1016/j.jhazmat.2006.01.012

Nomenclature

A	filter face area exposed to fluid flow (m^2)
A_S	Happel's parameter
D	diffusion coefficient (m^2/s)
d_c	mean collector size (m)
d_p	dust particle size (m)
E_{over}	overall collection efficiency
E_{frac}	fractional collection efficiency
F_S	Cunningham slip factor
G	gravity acceleration (m/s^2)
K_B	Boltzmann's constant ($kg\,m)/(s^2\,K$)
K	dimensionless parameter defined in Eq. (9)
k_1	Darcian permeability constant (m^2)
k_2	non-Darcian permeability constant (m)
L	filter thickness (m)
M_i	mass of particles in a given size range sampled at the filter entrance (kg)
M_o	mass of particles in a given size range sampled at the filter exit (kg)
N_i	Number of particles in a given size range sampled at the filter entrance
N_o	Number of particles in a given size range sampled at the filter exit
N_{Pe}	Peclet's number
N_{Re}	Reynolds' number
N_{St}	Stokes' number
$N_{St\,eff}$	effective Stokes' number
P	absolute pressure ($kg/m\,s^2$)
P_i	absolute inlet pressure ($kg/m\,s^2$)
P_o	absolute outlet pressure ($kg/m\,s^2$)
T	absolute temperature (K)
v_s	fluid velocity or filtration velocity (m/s)
v_t	terminal settling velocity (m/s)

Greek symbols

α_1–α_4	fitting constants in Eq. (23)
ε	porosity of the filter
γ	probability of adhesion
η_D	single collector efficiency due to diffusion
η_{DI}	single collector efficiency due to direct interception
η_E	single collector efficiency due to electrophoresis
η_G	single collector efficiency due to gravity
η_I	single collector efficiency due to inertia
η_T	total single collector efficiency
λ	mean free path of gas molecules (m)
μ_{air}	absolute air viscosity ($kg/m\,s$)
ρ_{air}	air density (kg/m^3)
ρ_p	dust particle density (kg/m^3)

constituents: fibrous filters and granule-bonded filters. Fibrous ceramic filters are made of alumina, aluminosilicates or zirconia filaments ranging from 2 to 20 μm in diameter. They have high porosity ($\varepsilon \cong 80$–95%), specific surface area ($S_o \cong 0.8$–$1.5 \times 10^6\ m^2/m^3$) and permeability ($k_1 \cong 10^{-15}$ to $10^{-10}\ m^2$). Their collection efficiency is very high and the pressure drop low, but they suffer from relatively low mechanical strength.

Granular filters, on the other hand, are made of alumina, silicon carbide, aluminosilicates, silica, mullite granules or a combination of them stuck together by ceramic binders. Similarly to fibrous filters, they can withstand hostile atmospheres and high temperatures and pressures. Their porosity ranges between 40–60%, giving a good mechanical strength but a relatively low permeability [13,14].

In recent years, a new category of ceramic filter has gained ground: the double-layered filters [15–17]. Each layer can be optimized according to the desired requirements, combining in one product the best features of both fibrous and granular filters. The support layer is made of a highly porous ceramic foam, which provides good mechanical integrity, resistance to thermal cycling and almost no resistance to gas flow [18]. The filtering layer, on the other hand, is made of a thin granular membrane deposited on one surface of the support layer, providing a physical barrier to collect small particles with a minimum pressure drop [2,3].

The objective of this work is to investigate the performance of a double-layered filter for aerosol filtration at high temperatures. Laboratory tests included measurement of permeability and fractional collection efficiency in different temperatures and filtration times.

2. Experimental procedure

2.1. Sample preparation

Ceramic supports were prepared by the replication technique from the impregnation of a ceramic slurry of water, alumina (A3000FL, Alcoa, Brazil) and dispersant (Darwan 7s) into polyurethane foam matrices (Bulpren R, Sidney Heath & Son, Stoke-on-Trent, UK) of 45 and 75 pores per linear inch (ppi). Support samples, disks with diameter of 6.6 cm and thickness of about 1.8 cm, were sintered in an electric furnace at 1600 °C for 2 h.

The filtering layer was prepared from a ceramic paste, consisted of 20 wt% water and 80 wt% solids (75 wt% fused alumina (+80–70 mesh), 25 wt% ball clay (−200 mesh) and sodium silicate as binder. The ball clay utilized (São Simão) had approximately 45% of SiO_2, 33.5% Al_2O_3, 1.5%Fe_2O_3 and 1.3% TiO_2 [19].

One millimeter of paste was deposited on one face of each sintered support and then the whole structure was dried and heated to 1400 °C to provide a good adhesion of both layers. The heating procedure was as follows:

- oven at ambient pressure and open to the atmospheric air;
- heating rate of 2 °C/min;
- 120 min at 700 °C;
- 120 min at 1400 °C.

Fig. 1 shows a SEM micrograph of the cross section of a 75 ppi filter utilized in this work.

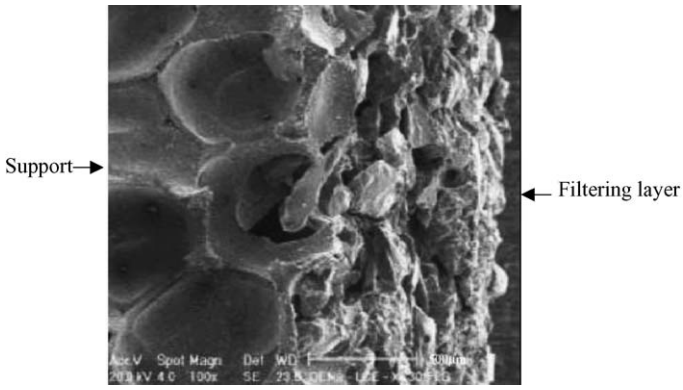

Fig. 1. SEM micrograph (100×) of the double-layered filter in the interface between the 75 ppi support and the filtering layer.

2.2. Characterisation tests

Ceramic supports were characterized according to their pore size distribution by image analysis (Image pro-plus 3.0 for Windows), porosity and air permeability at room and high temperatures. The bed porosity, ε, was estimated by the expression $\varepsilon = (1 - \rho_b/\rho_s)$, where ρ_b is the overall density of the ceramic body (determined by measuring the mass of a known body volume) and ρ_s is density of the solid material used for manufacturing the ceramic body (measured with a helium picnometer Micromeritcs Accupic). The double-layered filters were characterized by SEM (Philips XL30 FEG), air permeability and filtration efficiency at 25, 300 and 700 °C.

The filtration device consisted of two cylindrical chambers made of refractory stainless steel (service temperature up to 870 °C). A cylindrical sample-holder made of refractory stainless steel with a low thermal-expansion coefficient was fixed between the chambers by stainless steel bolts. Sample size was typically 6.6 cm in diameter (3 cm exposed to air flow and 3.6 cm to support the sample) and 1.8 cm thick. The test specimen was tightly fixed in the sample-holder using heat-resistant O-rings to avoid leakage. The entire system (chambers and sample-holder) was set within an electric furnace (Maitec, 7500 W) controlled by a PID system (Flyever). Dry air, supplied by a compressor (1500 W) and heated according to a preset program within the electric furnace, was allowed to flow from the bottom to the upper chamber.

Temperature was monitored with K-type thermocouples located in the entrance and exit chambers and also inside the furnace. Air pressure measurements were taken in both chambers using an electronic micromanometer (Furness Control Ltd.—FCO14). Air flow measurements were carried out with an electronic mass flow controller (Aalborg GFC-37).

The testing aerosol consisted of a phosphatic rock powder dispersed into the inlet air stream through a fluidized bed aerosol generator (TSI-2300). This generator consists of a bed of fluidized copper beads which is continuously fed by particles through a conveying belt situated on the lower region of the bed. A previous work [2] showed that this powder undergoes no chemical or thermal change up to 1000 °C. Typical aerosol concentration in tests was 0.014 g/m^3. Table 1 gives the features of the tested dust. Fig. 2a illustrates the device for permeability and filtration experiments, which is schematically shown in Fig. 2b.

Table 1
Particle size distribution of tested dust

Particle size (μm)	Mass percentage (wt%)
0.40	0.17
0.75	1.01
1.5	4.83
2.5	9.56
3.5	18.47
4.5	26.99
6.0	23.60
8.5	15.36

Particle density (ρ_p): 2970 kg/m^3; Sauter average mass diameter: 3.87 μm.

For permeability evaluation of samples, fluid velocity varied from 0 to about 1 m/s, and values were corrected according to ideal gas law for each test temperature. For filtration tests, actual fluid velocity was fixed at 0.10 m/s. Evaluation of collection efficiency started 10 min after the beginning of the test, with the introduction of aerosol in the system. The number of particles in the air stream was monitored in eight different sizes (0.4, 0.75, 1.5, 2.5, 3.5, 4.5, 6.0 and 8.5 μm) at the inlet and outlet of the filter. The duration of each sampling was 1 min. Another particle counting was made after 20 min of operation to verify the effect of the filtration time on the filter performance. The whole procedure was then repeated for each testing temperature with a new virgin filter.

Permeability data for the support and clean filters were fitted to Forchheimer's Eq. [20] for compressible fluids [18]:

$$\frac{P_i^2 - P_o^2}{2P_iL} = \frac{\mu_{air}}{k_1}v_s + \frac{\rho_{air}}{k_2}v_s^2 \quad (1)$$

in which L is the sample thickness along the flow direction, P_i and P_o are the absolute air pressures at the medium inlet and outlet, respectively. μ_{air} and ρ_{air} are, respectively, the absolute viscosity and the density of the air, and v_s is the fluid velocity, determined by $v_s = Q/A$, where Q is the volumetric flow rate and A is the exposed surface area of the sample perpendicular to flow direction. k_1 and k_2 are usually known as Darcian and non-Darcian permeability constants, in reference to Darcy's law. These parameters incorporate only the structural features of the porous medium and therefore are considered constant at a given temperature even if changing the fluid or the flow conditions.

Fluid properties ρ_{air} and μ_{air} were corrected according to the test temperature T and average pressure P ($(P_i + P_o)/2$) by the following expressions [2]:

$$\rho_{air} = \frac{3.488 \times 10^{-3}P}{T} \quad (2)$$

$$\mu_{air} = 1.73 \times 10^{-5}\left(\frac{T}{273}\right)^{1.5}\left(\frac{378}{T + 125}\right) \quad (3)$$

in which T, P, μ_{air} and ρ_{air} are given in S.I. units.

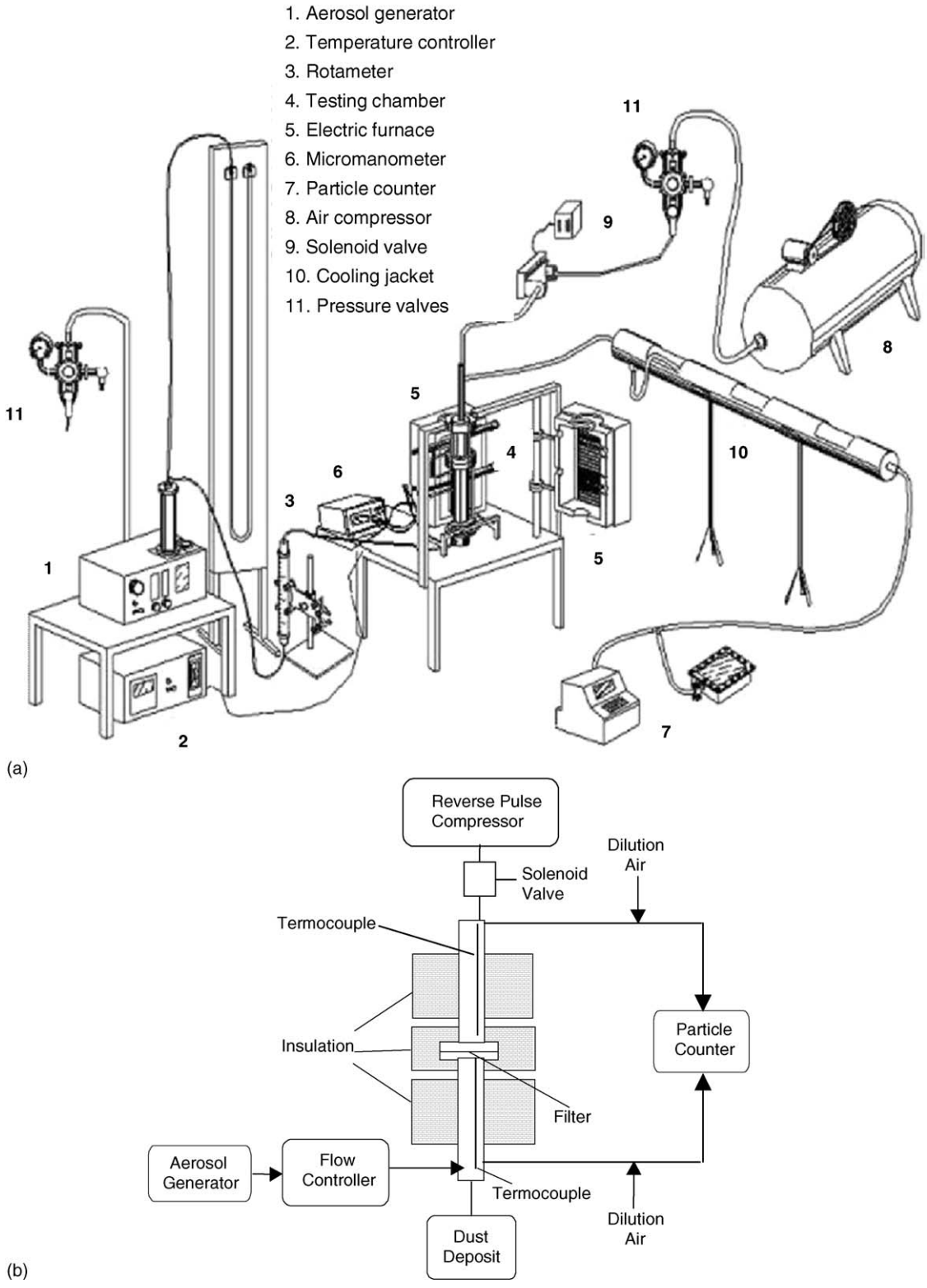

Fig. 2. Permeability and filtration rig at room and high temperatures: (a) overall view; (b) schematic view of the main components.

Fractional collection efficiency in each particle size range (E_{frac}) was calculated by:

$$E_{frac} = \frac{N_i - N_o}{N_i} \quad (4)$$

in which N_i and N_o are the number of particles measured by periodical sampling, respectively, at the inlet and outlet of the filter for each size range. The particle counter utilized was the Hiac/Royco, model 5230. As the aerosol sampling flow rate of this equipment was higher than the range utilized in the filtra-

tion tests, there was no need for isokinetic sampling. During the sizing tests, the whole dust laden gas was sucked into the equipment, together with clean air for completing the sampling flow rate.

3. Results and discussion

Features of the support layers prepared in this work are presented in Table 2. The ceramic supports prepared from 45 ppi foams were more porous and with a higher pore size than the one based on 75 ppi foams. In both cases, however, a suitable permeability level for hot gas filtration was achieved. As comparison, Seville et al. [21] found permeability values (k_1) for fibrous ceramic elements of very high porosity ($\varepsilon \cong 0.8$–0.95) varying from 0.4 to 4.8×10^{-11} m^2. Innocentini [2] worked with airflow through a similar commercial fibrous medium ($\varepsilon \cong 0.8$) and determined average experimental values for k_1 and k_2 as 1.72×10^{-11} m^2 and 2.04×10^{-6} m, respectively.

3.1. The permeability

Fig. 3 compares the permeability behavior of filters with different support layers as a function of temperature. A linear relationship was found between the Darcian permeability k_1 and the test temperature. A similar behavior was already reported in the literature and the explanation was related to the thermal expansion of the filter structure, which causes the temporary opening of porous channels to fluid flow [2,22,23]. As expected, the 45 ppi filter was slightly more permeable than the 75 ppi filter, indicating the small contribution of the ceramic foam supports for the total pressure drop across the filters.

Table 2
Features of ceramic foam supports

Nominal pore count (ppi)	Porosity	Mean pore size (mm)	k_1[a] (10^{-9} m^2)	k_2[a] (10^{-4} m)
45	0.797 ± 0.013	0.546 ± 0.045	7.29	2.78
75	0.741 ± 0.025	0.266 ± 0.058	2.26	1.47

[a] Values obtained at room temperature.

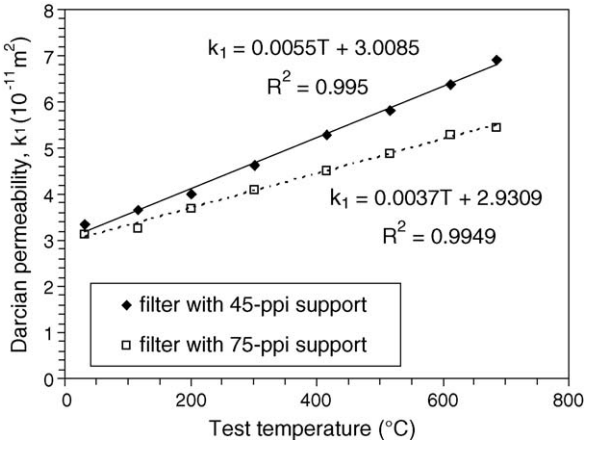

Fig. 3. Darcian permeability constants (k_1) as a function of test temperature for the different filters tested in this work. R^2 is the correlation coefficient for the data.

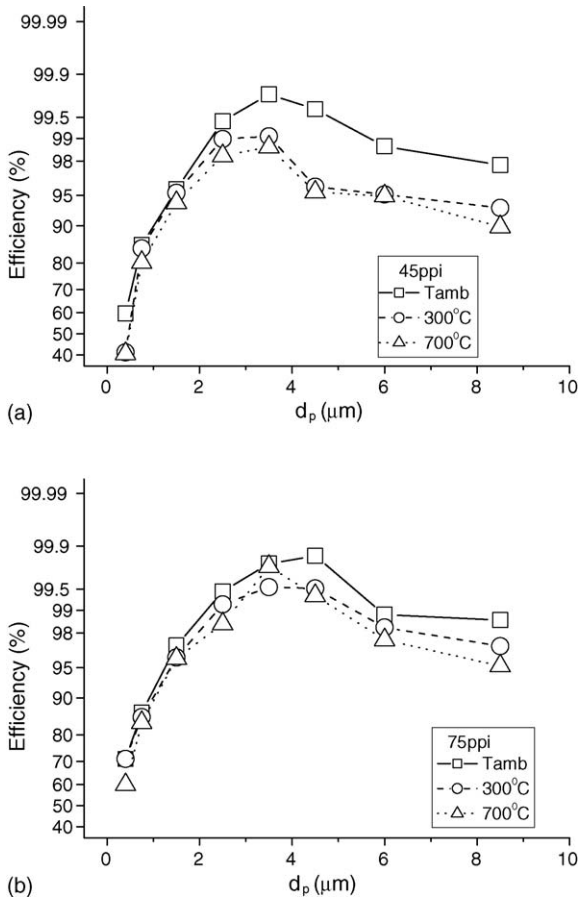

Fig. 4. Collection efficiency as a function of particle size for a clean filter, at the three temperatures investigated: (a) support of 45 ppi and (b) support of 75 ppi.

3.2. The collection efficiency

The curves of fractional collection efficiency for the different experimental conditions are given in Figs. 4 and 5. It is apparent that the filter efficiency decreases with the increase of the gas temperature in all tests performed. Part of this effect can be explained by the variation of the gas physical properties with temperature. But structural changes in the filter medium (thermal expansion) may also play a role in this behavior, as the existing correlations do not predict the temperature variation correctly and needed modification (see the modeling section below).

Fig. 4 refers to the initial stages of filtration. It is observed that efficiency increases with increasing particle size, for particles up to 3 μm, probably due to the inertial collection mechanism (see the modeling section below). However, collection was not necessarily better for larger dust particles. In fact, efficiency reached a maximum for particles between 2 and 4 μm. Below this range, penetration of small particles through the filter was considerable and efficiency was relatively low in all temperatures and filters tested: between 40 and 95% for the 45 ppi filter. A comparison between Fig. 4a and b shows that the performance of the 75 ppi filter is better (efficiencies between 60 and 95% in the same

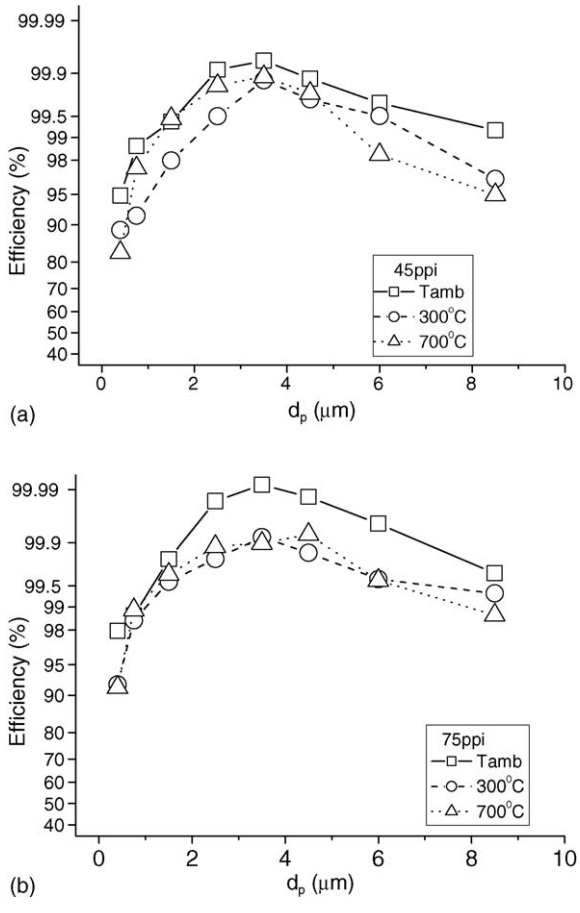

Fig. 5. Collection efficiency as a function of particle size for a filter after 20 min of operation, at the three temperatures investigated: (a) support of 45 ppi and (b) support of 75 ppi.

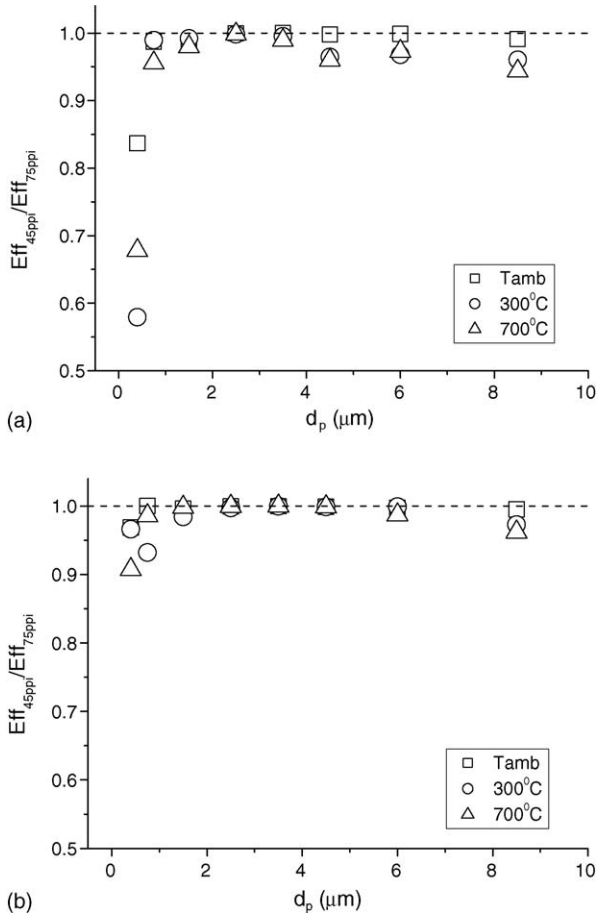

Fig. 6. Relative values of the collection efficiency for the two supports tested ($Eff_{45\,ppi}/Eff_{75\,ppi}$) as a function of particle diameter at the three temperatures investigated: (a) clean filter and (b) after 20 min of filtration.

size range), demonstrating that the highly porous support has effect on the filtration behavior. It is also clearly noticeable in Figs. 4 and 5 that the efficiency decreased for particles between 4 and 8 μm. This decrease is probably due to particle bouncing or re-entrainment after collection. Nevertheless, it is expected that efficiency eventually increases for particles somewhat larger than 8 μm, as particle screening becomes important.

Fig. 5a and b show the filter performance after 20 min of operation for the 45 and 75 ppi filers, respectively. During this time, an amount of particles has been collected and their effect on the filter behavior explains the observed increase in the collection efficiency in both filters. It is worth noting that, considering the particle concentration in the air, the filter area and the operation time, the amount of deposited particles at the end of 20 min was of the order of 0.15 mg/cm^2 of filter. Although very small, this amount of particles promotes the observed increase in the filter efficiency, but at a cost: the pressure drop across the membrane also increases substantially, leading to the necessity of a periodical cleaning of the medium.

3.3. The pore size

Fig. 6 shows the effect of pore size of the structural (foam) layer in the filter performance. The filter with larger pore sizes (45 ppi) exhibits smaller efficiencies in all the size range investigated, but this better performance is maximized for the particles smaller than 2 μm in diameter in the initial stages of the filtration (see Fig. 6a). As the process proceeds, the two filters tend to the same efficiency (see Fig. 6b). It is worth remembering that the structural (foam) layer, highly porous, was used only as support for the filtering layer, which was identical in both filters.

3.4. The filtration time

The effect of the filtration time can be more clearly seen in Fig. 7. Again, the smaller particles are more sensitive to the parameter. The collection efficiency of the particles below 1 μm in diameter practically doubles after 20 min of filter operation in the 45 ppi filter (see Fig. 7a), whereas increases 1.5 times in the 75 ppi filter (see Fig. 7b). This improvement is certainly due to the collected particles that, once deposited on the filtering layer, start to act as collectors of the subsequent particles, eventually forming an independent layer known as filter 'cake'. As already mentioned, this cake increases the filter pressure drop, and has to be periodically removed. The filter performance in these circumstances is presented elsewhere [24].

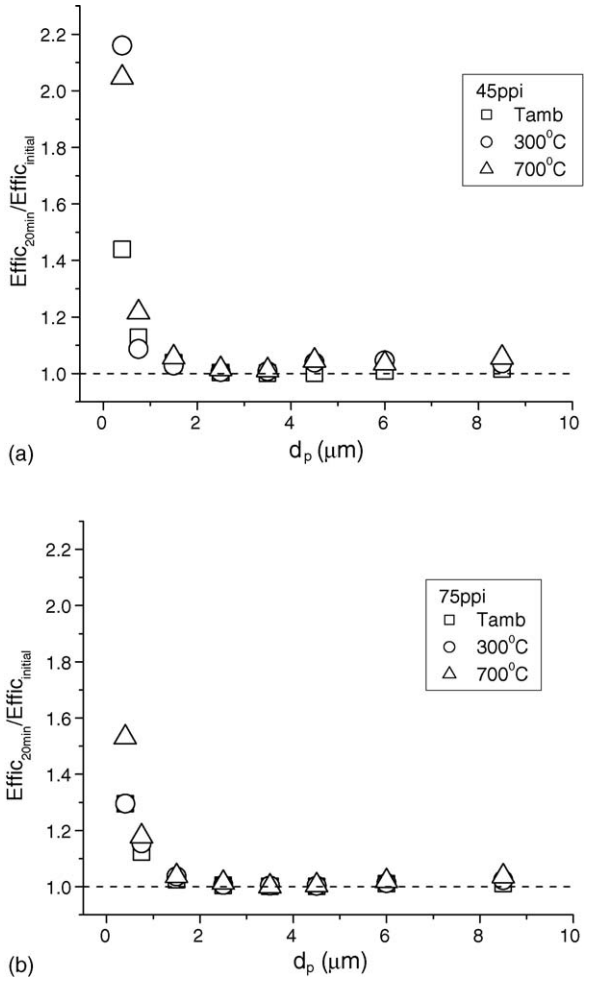

Fig. 7. Relative values of the collection efficiency at different filtration times ($Eff_{20\,min}/Eff_{initial}$) as a function of particle diameter at the three temperatures investigated: (a) support of 45 ppi and (b) support of 75 ppi.

3.5. A correlation for the collection efficiency

The observed behavior for the fractional efficiency was analyzed according to the several collection mechanisms occurring in a barrier filter. The expressions derived in the literature were based on semi-empirical correlations and the process was considered to be time-independent, valid for the first stages of filtration when no dust cake is present in the filter. In this work, the modeling of fractional efficiency of the filter was based on the single collector efficiency model [25,26]:

$$E_{frac} = 1 - \exp\left[-\frac{aKL(1-\varepsilon)\eta_T}{d_c}\right] \quad (5)$$

in which L is the thickness of the filtering layer, a a fitting constant ($a = 46.4$) and d_c is the diameter of a single collector (considered in this work as the maximum alumina particle size, $d_c = 246\,\mu m$, obtained by image analysis). Units are given in the S.I.

In this work, the filter porosity ε was experimentally related to the testing temperature according to the following expressions:

$$\varepsilon = 0.330 + 9.77 \times 10^{-5} T, \quad \text{for the 45 ppi filter} \quad (6)$$

$$\varepsilon = 0.325 + 7.49 \times 10^{-5} T, \quad \text{for the 75 ppi filter} \quad (7)$$

The parameter K was proposed by Yoshida and Tien [27] as:

$$K = \left[\frac{6}{(1-\varepsilon)^{2/3}}\right]^{1/3} \quad (8)$$

According to this model, the total collection efficiency of a single collector (η_T) can be approximated by the sum of its individual efficiencies due to different mechanisms: diffusion (D), inertia (I), direct interception (DI), gravity (G) and electrophoresis (E). In this work, the original expression was modified to take into account the probability of retention of a particle on the collector (γ): The expression for η_T then becomes:

$$\eta_T = \gamma(\eta_D + \eta_I + \eta_{DI} + \eta_G + \eta_E) \quad (9)$$

Diffusional collection arises from the random movement to which small particles are subjected in a gas, known as Brownian diffusion. Tien [25] proposed the following correlation for estimation of single efficiency according to this mechanism:

$$\eta_D = 4(1-\varepsilon)^{2/3} A_S^{1/3} N_{Pe}^{-2/3} \quad (10)$$

in which the Happel's parameter (A_S) and the Peclet's number (N_{Pe}) are, respectively, given by:

$$A_S = \frac{2[1-(1-\varepsilon)^{5/3}]}{2-3(1-\varepsilon)^{1/3}+3(1-\varepsilon)^{5/3}-2(1-\varepsilon)^2} \quad (11)$$

$$N_{Pe} = \frac{v_s d_c}{D} \quad (12)$$

in which v_s is the filtration velocity and the D diffusion coefficient, estimated by:

$$D = \frac{K_B T F_s}{3\pi\mu_{air} d_p} \quad (13)$$

here K_B is the Boltzmann's constant ($1.380622 \times 10^{-23}\,J\,K^{-1}$), T the absolute temperature, d_p the dust particle size and μ_{air} the air viscosity. The slip factor F_s was given by Allen and Raabe [28] as:

$$F_s = 1 + \frac{\lambda}{d_p}\left[2.34 + 1.05\exp\left(-0.39\frac{d_p}{\lambda}\right)\right] \quad (14)$$

in which λ is the mean free path of the molecules in the gas and d_p is the dust particle size.

Inertia also contributes for collection efficiency. The gas streamlines curve to pass around the collector, and the ability of a particle to follow the streamlines decreases with increasing mass of the particle. This mechanism dominates at high velocities, but particle bouncing must be necessarily taken into account. The expression proposed by Jung et al. [29] was chosen here to represent this mechanism:

$$\eta_I = 0.2589 \times N_{St\,eff}^{1.3437} N_R^{0.23} \quad (15)$$

in which N_R and $N_{St\,eff}$ are, respectively, the interception parameter and the effective Stokes number, given by:

$$N_R = \frac{d_p}{d_c} \tag{16}$$

$$N_{St\,eff} = [A_S + 1.14 N_{Re}^{0.5} \varepsilon^{-1.5}] \frac{N_{St}}{2} \tag{17}$$

where N_{Re} is the Reynolds number, given by:

$$N_{Re} = \frac{\rho_{air} v_s d_c}{\mu_{air}} \tag{18}$$

The Stokes number (N_{St}) is expressed by:

$$N_{St} = \frac{\rho_p d_p^2 v_s F_s}{9 \mu_{air} d_c} \tag{19}$$

On the other hand, the direct interception mechanism arises from the fact that the particle has a finite size. If its centre passes within a distance of $d_p/2$ from the collector surface, then particle is collected. The expression developed by Paretsky et al. [30] was used for estimation of the direct interception effect on particle collection:

$$\eta_{DI} = 6.3 \varepsilon^{-2.4} N_R^2 \tag{20}$$

Gravitational collection results from the action of gravity on the dust particle, which causes its trajectory to deviate from the gas streamlines. This mechanism may become the dominant process at low gas velocities, for particles large enough to have significant terminal velocity and very small Brownian diffusivity. The efficiency depends on the flow direction and is higher for downward filtration. The relationship used here for the gravitational collection was based on upward flow as [30,31]:

$$\eta_G = 3.75 \times 10^{-2} \left(\frac{v_t}{v_s} \right)^{0.5} \tag{21}$$

in which v_t is the terminal settling velocity of the dust particle, obtained within the Stokes free-fall regime ($N_{Re} < 1$) by:

$$v_t = \frac{\rho_p d_p^2 g}{18 \mu_{air}} \tag{22}$$

Electrophoretic collection results from the presence of electrostatic charges on the particles, collectors or both. These charges are generated either by phenomena inherent in the process (e.g. triboelectrification) or deliberately introduced (by corona charging, for example) [26]. In this work, electrophoretic efficiency expressions were not considered due to the lack of data on electrostatic charges at high temperatures.

The probability of retention of a particle on the single collector (γ) was investigated by Yoshida and Tien [27], who observed that the collection efficiency decreased with increasing Stokes' number (N_{St}) due to particle bouncing or re-entrainment. Tien [25] proposed that γ could be better represented as a function of an effective Stokes' number ($N_{St\,eff}$), whereas Cavenati and Coury [32] incorporated the influence of filter dimensions on such parameter. Based on those studies, the present authors propose a modified version of the γ parameter, represented by Eq. (23).

$$\gamma = \alpha_1 \left(\frac{L}{D} \right)^{\alpha_2} N_{Re}^{\alpha_3} N_{St\,eff}^{\alpha_4} \tag{23}$$

In the present work, values for constants α_1–α_4 were fitted to experimental data (least square deviation between predicted decrease in collection efficiency due to bouncing/re-entrainment and the experimental values) and the following correlation was found:

$$\gamma = 0.000441 \times \left(\frac{L}{D} \right)^{-0.228} N_R^{-1.197} N_{St\,eff}^{-1.057} \tag{24}$$

with γ limited between 0 and 1.

Expressions for diffusional, gravitational, direct interception and inertial collection mechanisms, given by Eqs. (5)–(24), were combined to finally estimate the efficiency of the filter for each dust particle range according to the studied operational conditions (Eq. (5)). Comparison of modeling and experiments are given in Fig. 8.

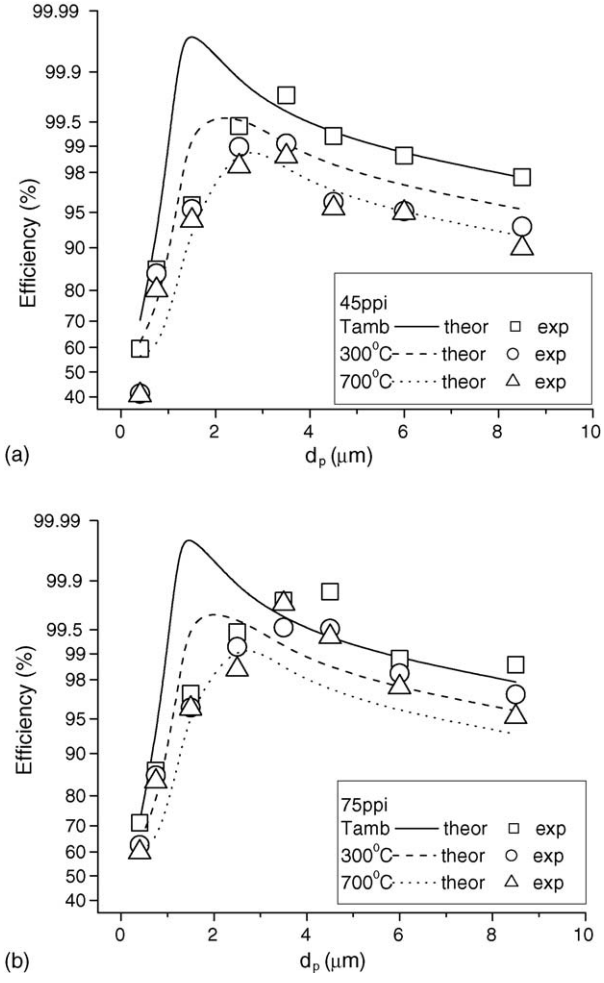

Fig. 8. Comparison between modeling and experimental curves of fractional collection efficiency at the three temperatures investigated for (a) the support of 45 ppi and (b) the support of 75 ppi.

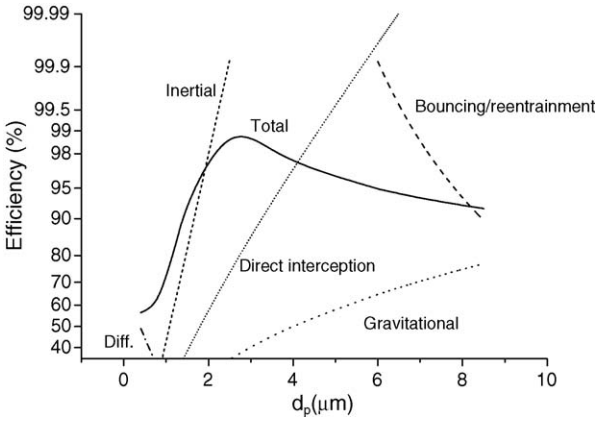

Fig. 9. Theoretical predictions for the filter efficiency due to each of the individual mechanisms assumed in the model. Curves obtained for 45 ppi and 700 °C.

Curves in Fig. 8 reveal a satisfactory agreement between experimental fractional efficiencies and the proposed correlation. Fig. 9 illustrates the contribution of the assumed mechanisms in the formation of the final theoretical curve. It can be seen that the efficiency behavior for particles below 2 μm is mainly due to the inertial mechanism while in the range of 4–8 μm the bouncing/re-entrainment predominates as detachment mechanisms. It is worth noting that the discrepancy between the model and the data in the 2 μm region was enhanced by the probability coordinate adopted for the y axis. In reality, the difference is never higher than 0.45%.

4. Conclusions

A double-layered ceramic filter was developed and tested for use for gas filtration at high temperatures. The filter was based on different ceramic foam supports and a thin granular filtering layer. Tests included measurement of porosity, permeability and filtration performance in temperatures ranging from ambient to 700 °C. Results showed that filters presented high collection efficiency, comparable to other ceramic filters reported in the literature. Fractional collection efficiency was sensitive to the gas temperature, to the structural (foam) layer and to filtration time. For similar experimental conditions, it decreased with the increase in temperature. Also, the efficiency was lower for particles below 2 μm and in the range 4–8 μm and explanation is based on the influence of different dust particle collection mechanisms. A correlation that estimates the fractional efficiency was proposed, being based on semi-empirical expressions available in the literature. Results showed satisfactory agreement between experimental data and the proposed correlation. They also revealed the particle inertia as the predominant collection mechanism within the studied range, with particle bouncing/re-entrainment acting as detachment mechanisms.

Acknowledgements

Authors would like to thank the Brazilian research funding institutions CNPq, CAPES and FAPESP.

References

[1] M.A. Alvin, Advanced materials for use in high-temperature particulate removal systems, Ind. Eng. Chem. Res. 35 (1996) 3384–3396.
[2] Innocentini, M.D.M. Aerosol filtration at high temperatures, Doctorate Thesis, Federal University of São Carlos, Brazil, 1997 (in Portuguese).
[3] N.L. Freitas, M.G. de Maniero, J.R. Coury, Filtration of aerosols at high temperatures using a double layer ceramic filter: influence of the particle diameter in the collection efficiency, Cerâmica 50 (October/December) (2004) 355–361 (available at www.scielo.br).
[4] US-EPA, National Ambient Air Quality Standards (NAAQS), 1990 (available at http://epa.gov/air/criteria.html).
[5] D. Fino, G. Saracco, V. Specchia, Filtration and catalytic abatement of diesel particulate from stationary sources, Chem. Eng. Sci. 57 (2002) 4955–4966.
[6] G. Saracco, C. Badini, V. Specchia, Catalytic traps for diesel particulate control, Chem. Eng. Sci. 54 (1999) 3035–3041.
[7] M. Ambrogio, Saracco, V. Specchia, C. van Gulijk, M. Makkee, J.A. Moulijn, On the generation of aerosol for diesel particulate filtration studies, Sep. Purif. Technol. 27 (2002) 195–209.
[8] M. Ambrogio, Saracco, V. Specchia, Combining filtration and catalytic combustion in particulate traps for diesel exhaust treatment, Chem. Eng. Sci. 56 (2001) 1613–1621.
[9] W. de Wong, O. Unal, J. Andries, K.R.G. Hein, H. Spliethoff, Biomass and fossil fuel conversion by pressurized fluidized bed gasification using hot gas ceramic Filters as gas cleaning, Biomass Bioenergy 25 (1) (2003) 59–83.
[10] G. Ahmadi, D.H. Smith, Gas flow and particle deposition in the hot-gas filter vessel of the Pinon Pine Project, Powder Technol. 128 (1) (2002) 1–10.
[11] H. Sasatsu, N. Misawa, M. Shimizu, R. Abe, Predicting the pressure drop across hot gas filter (CTF) in a commercial size PFBC system, Powder Technol. 118 (1–2) (2001) 58–67.
[12] C.N. Hamelink, A.P.C. Faaij, Future prospects for production of methanol and hydrogen from biomass, J Power Sources 111 (1) (2002) 1–22.
[13] M.A. Alvin, T.E. Lippert, J.E. Lane, Assessment of porous ceramic materials for hot gas filtration applications, Ceram. Bull. 70 (9) (1991) 1491–1498.
[14] P.M. Eggerstedt, J.F. Zievers, E.C. Zievers, Choose the right ceramic for filtering hot gases, Chem. Eng. Prog. January (1993) 62–69.
[15] J.P.K. Seville, S. Ivatl, G.K. Burnard, Recent advances in particulate removal fro hot process gases, in: E. Schmidt (Ed.), High Temperature Gas Cleaning, vol. I, Karlsruhe, 1996, pp. 3–25.
[16] Y. Kinemnuchi, T. Suzuki, W. Jiang, K. Yatsui, Ceramic membrane filter using ultrafine powders, J. Am. Ceram. Soc. 84 (9) (2001) 2144–2146.
[17] R.K. Ahluwalia, H.K. Geyer, Fluid mechanics of membrane-coated ceramic filters, Trans. ASME 118 (July) (1996) 526–533.
[18] E.A. Moreira, M.D.M. Innocentini, J.R. Coury, Permeability of ceramic foams to compressible and incompressible flow, J. Eur. Ceram. Soc. 24 (10–11) (2004) 3128–3209.
[19] J.F.M. Motta, L.C. Tanno, M. Cabral Jr., Ball and plastic clays in the State of São Paulo—geological features, Revista Brasileira de Geociências 23 (2) (1993) 158–173 (available at www.scielo.br).
[20] P.H. Forchheimer, Wasserbewegung durch Boden, Z. Ver. Deutsch Ing. 45 (1901) 1782–1788.
[21] J.P.K. Seville, R. Clift, C.J. Withers, W. Keidel, Rigid ceramic media for filtering hot gases, Filtr. Sep. July/August (1989) 265–271.
[22] M.D.M. Innocentini, W.L. Antunes, J.B. Baumgartner, J.P.K. Seville, J.R. Coury, Permeability of ceramic membranes to gas flow, Mater. Sci. Forum 299/300 (1999) 19–28.
[23] M.D.M. Innocentini, M.G. Silva, B.A. Menegazzo, V.C. Pandolfelli, Permeability of refractory castables at high-temperatures, J. Am. Ceram. Soc. 84 (3) (2001) 645–647.

[24] Freitas, N.L. de, Gonçalves, J.A.S., Innocentini, M.D.M., Coury, J.R., Aerosol filtration at high-temperatures using double-layered ceramic filters: II- operational behavior, in preparation.
[25] C. Tien, Granular Filtration of Aerosol and Hydrosols, Butterworths, USA, 1989.
[26] Coury, J.R., Electrostatic effects in granular bed filtration of gases, Ph.D. Thesis, University of Cambridge, UK, 1983.
[27] H. Yoshida, C. Tien, A new correlation of the initial collection efficiency of granular aerosol filtration, AIChE J. 31 (10) (1985) 1752–1754.
[28] M.D. Allen, O.G. Raabe, Slip correction measurements of spherical solid aerosol particles in an improved Millikan apparatus, Aerosol Sci. Technol. 4 (1985) 269–286.
[29] Y. Jung, S.A. Walata, C. Tien, Experimental determination of the inicial collection efficiency of granular beds in the inertial-impaction-dominated region, Aerosol Sci. Technol. 11 (1989) 168–182.
[30] L. Paretsky, L. Theodore, R. Pfeffer, A.M. Squires, Panel bed filters for simultaneous removal of fly ash and sulphur dioxide. 2: Filtration of Dilute aerosols by sand beds, J.A.P.C.A. 21 (4) (1971) 204.
[31] J.R. Coury, K.V. Thambimuthu, R. Clift, Capture and rebound of dust in granular bed filters, Powder Technol. 50 (1987) 253–265.
[32] S. Cavenati, J.R. Coury, Particle bouncing in granular bed filtration of gases, in: Proceedings of the World Congress on Particle Technology, vol. 3, Brighton, July, 1998.